ADVANCEMENTS IN FREE SURFACE RANSE SIMULATIONS FOR SAILING YACHT APPLICATIONS

Christoph Böhm, Delft University of Technology, NL / Yacht Research Unit Kiel, GER, christoph.boehm@yru-kiel.de
Kai Graf, University of Applied Sciences Kiel, GER / Yacht Research Unit Kiel, GER, kai.graf@fh-kiel.de

The analysis of yacht hulls performance using RANSE based free surface simulations has become an accepted approach over the last decade. Access to this technology has been eased by the development of user-friendly software and by the increase of computational power. Results are widely accepted as superior to previous non-viscous approaches and have to compete with towing tank results in terms of accuracy. However, many practical applications suffer from a numerical smearing of the free surface interface between air and water which can be described as numerical ventilation. This problem occurs when the intersection between bow and calm water surface form an acute angle and is further pronounced if the stem is rounded or blunt. It is therefore especially linked to sailing yacht applications. The problem manifests itself as a non-physical suction of the air-water mixture under the yacht hull, causing a significant underprediction of viscous resistance. While this is the easily observable appearance of the problem, a second issue is its effect on wave resistance. It can be shown that wave damping is significantly increased, causing a prediction of wave resistance which is also too low. The paper provides a review of the Volume-of-Fluid method. It discusses the resultant implications for practical applications. A remedy to circumvent the problem is described and its impact on the accuracy of the result is shown. Simulations on an identical appended hull with and without interface smearing are compared. Effects on free surface visualization and numerical accuracy are shown. The paper finishes with a thorough verification and validation of a fully appended yacht in accordance with ITTC standards.

NOMENCLATURE

$(1+k)$	Form factor	(-)
CFL	Courant number	(-)
C_D	Drag coefficient	(-)
C_L	Lift coefficient	(-)
C_T	Total resistance coefficient	(-)
C_k	Correction factor	(-)
E	Comparison error	(-)
Fn	Froude number	(-)
P_k	Order of accuracy	(-)
R_k	Convergence ratio	(-)
Rn	Reynolds number	(-)
S	Simulation results	(-)
T	Truth	(-)
U_{SN}	Numerical uncertainty	(-)
U_P	Parameter uncertainty (e.g. iteration number $_I$, grid size $_G$, time step $_T$)	(-)
V	Volume	(m^3)
α_i	Volume fraction of fluid i within a cell	(-)
$\delta_k^\star$	error estimate with sign and magnitude of kth parameter	(-)
δ_p	Parameter error (e.g. iteration number $_I$, grid size $_G$, time step $_T$)	(-)
δ_S	Simulation error	(-)
δ_{SM}	Simulation modeling error	(-)
δ_{SN}	Simulation numerical error	(-)
ϵ_{ijk}	Solution change	(-)
λ	Scale factor	(-)
$\mathbf{S}$	Surface vector	(m^2)
$\mathbf{n}$	Surface normal vector	(-)
$\mathbf{v}$	velocity vector	($m.s^{-1}$)
$\mathbf{v}_b$	grid velocity vector	($m.s^{-1}$)
$\tilde{\phi}_C$	normalized value of central node w.r.t. face f	(-)
$\tilde{\phi}_C$	normalized face value	(-)
r_k	refinement ratio of parameter k	(-)

Subscripts

$_f$	Cell face
$_C$	Corrected error or uncertainty

1 Introduction

During the last decade RANSE based viscous free surface simulations around ship hulls have gained a certain degree of maturity. Their capability to produce reliable data which

can compete with towing tank experiments has been proved, e.g. by the Gothenburg 2010 Workshop on Ship Hydrodynamics [5]. The rapidly developing availability of computational power has increased the popularity of this kind of CFD technology and the access to it has been eased by software packages which guide the user through the pre-processing procedure. The once time-consuming procedure of creating a computational grid has been improved by new meshing techniques which can reliably handle complex geometries and allow to tailor the mesh such that it meets the special needs of ship hydrodynamics. These advances in computational power and numerical techniques have changed the challenge in CFD towards achieving results that are within an expected uncertainty. As mentioned above, verifications and validations for ship hydrodynamics can be found in literature and benchmark cases including geometries are available. Unfortunately the same does not hold true for yacht hydrodynamics were validations are rare and usually non-public. This might change in the future since results and geometries of the Delft Systematic Yacht Hull Series (DSYHS) have recently become publicly available.

2 Motivation

An attempt of the authors to validate RANSE CFD against towing tank results of an *America's Cup Class Version 5* boat (ACCV5) [1] showed good results at time of publication. Resistance in non-lifting conditions was resolved to -6.2% of the Experimental Fluid Data (EFD), whilst lifting condition proved to be a problem with drag and lift deltas of -2.5% and 19% respective . With the above mentioned advancements in RANSE CFD these simulations have been repeated including more recent free surface modeling and body motion techniques and a larger and apparently better suited computational grid. However, the results did not reflect the expected improvements, indeed they were even worse than before with differences between CFD and EFD resistance curves of approximately -8%. This obviously led to the question why these behavior occurred. In general, single phase RANSE simulations tend to over-predict drag values if grid resolution is not sufficiently small. This behavior is not absolutely transferable to free surface ship flows, were a insufficient resolution of the wave pattern might also lead to an under-prediction of drag. Nonetheless, under-prediction of drag hints to look at modeling errors. Figure 1 illustrates the *volume fraction of water* values on the hull. Normally one would expect that these values are zero in the air region, one in the submerged area of the hull and between zero and one in a small region around the free surface interface. In the vicinity of a sharp interface, this region should not significantly extend over more than three cells. Figure 1 clearly shows that this not the case. Instead volume fractions are smeared over the complete hull, expect around the appendages and in their wake. This clearly indicates a behavior which is sometimes referred to as *numerical ventilation* but can be shown to be a smeared free surface interface. Due to the nature of the treatment of physical properties of flow phase within the VOF (Volume-of-Fluid) model, this will lead to smaller resistance values. It has to be highlighted that the interface smearing as described above has only been encountered for specific floating bodies. These bodies have in common that they share a rather blunt bow which forms a small, acute entrance angle with the waterline. For conventional vessel which normally have sharp bow with a right angle at the water line, this problem does not occur. It is therefore kind of yacht-specific.

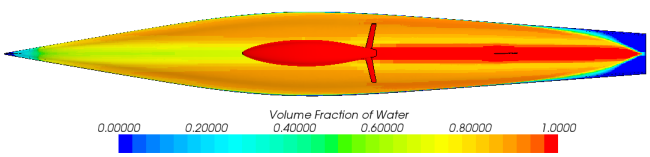

Figure 1: VOF

3 Volume-of-Fluid method

The Volume-of-Fluid (VOF) method was introduced by Hirts and Nicols [3]. It is an *Interface Capturing Methods without reconstruction* and thus does not treat the free surface as a sharp boundary. Instead the calculation is performed on a fixed grid, and free surface interface orientation and shape is calculated as function of the volume part of the respective fluid within a control volume (CV). The VOF method employs the concept of a equivalent fluid. This approach assumes that the (two) fluid phases share the same velocity and pressure fields allowing to solve the same set of governing equations describing momentum and mass transport as in a single phase flow. The Volume fraction α_i describes to which level the cell is filled with the respective fluid. The free surface is then defined as the isosurface at which the volume fractions take the value of 0.5. It is important to note, that this location is not at the control volume center but rather interpolated to the geometrical value. To simulate wave dynamics, one has to solve an equation for the filled fraction of each CV additionally to the conservation equations for mass and momentum. Assuming incompressible flow, the transport equation of volume fractions α_i is described by the following conservation equation:

$$\frac{\partial}{\partial t}\int_V \alpha_i \mathrm{d}V + \int_S \alpha_i \left(\mathbf{v} - \mathbf{v}_b\right)\cdot \mathbf{n}\mathrm{d}S = 0 \qquad (1)$$

The physical properties of the equivalent fluid within a control volume are then calculated as functions of the physical properties of the phases and their volume fractions. Strict conservation of mass is crucial, but this is easily obtained within this method as long as the sum of all volume-fractions per cell is 1. The critical issue for this kind of methods is the discretization of the convective term. Low-order terms like for instance 1st order upwind are known to smear the interface and introduce an artificial mixing of the two fluids. Therefore higher order schemes are preferred. The goal is to derive schemes which are able to keep the interface sharp and produce a monotone profile across it. Development of differencing schemes has been the pinnacle of research in the fields VOF methods for many years. Consequently a large

number of schemes is available and successfully used in different codes. The vast majority of these schemes is based on the Normalized Variable Diagram (NVD) and the Convection Boundedness Criterion (CBC) introduced by Leonard [6].

3.1 HRIC Scheme

The HRIC scheme (High Resolution Interface Capturing Scheme) is one of the most popular advection schemes and widely used in many CFD codes. It has been developed by Muzaferija and Peric [8, 10, 9]. Like most other schemes, it is based on a blending of bounded upwind and downwind schemes. The aim is to combine the compressive properties of the downwind differencing scheme with the stability of the upwind scheme. The bounded downwind scheme is formulated as:

$$\tilde{\phi}_f = \begin{cases} \tilde{\phi}_C & \text{if } \tilde{\phi}_C < 0 \\ 2\tilde{\phi}_C & \text{if } 0 \leq \tilde{\phi}_C \leq 0.5 \\ 1 & \text{if } 0.5 \leq \tilde{\phi}_C \leq 1 \\ \tilde{\phi}_C & \text{if } 1 \leq \tilde{\phi}_C \end{cases} \tag{2}$$

Since the amount of one fluid convected through a cell face shall be less or equal to the amount available in the donor cell, the calculated value of $\tilde{\phi}_f$ is corrected with respect to the local Courant number (CFL).The CFL is calculated by employing the the velocity at the cell face $\mathbf{v}_f$, the surface vector $\mathbf{S_f}$, the respective cell volume V_f and the local time step size dt as follows:

$$CFL = \frac{\mathbf{v}_f \mathbf{S_f} \mathrm{d}t}{V_f} \tag{3}$$

The correction takes the form of (4) and effectively controls the blending between HRIC and UD scheme with two limiting Courant numbers C_L and C_U which normally takes values of 0.5 and 1.0 respective 0.3 and 0.7.

$$\tilde{\phi}_f^* = \begin{cases} \tilde{\phi}_f & \text{if } CFL < 0 \\ \tilde{\phi}_C + \left(\tilde{\phi}_f - \tilde{\phi}_C\right) \frac{C_U - CFL}{C_U - C_L} & \text{if } C_L \leq CFL < C_U \\ \tilde{\phi}_C & \text{if } C_U \leq CFL \end{cases} \tag{4}$$

Effectively this correction implies that the HRIC scheme is used for a CFL smaller than the lower CFL limiter and UD scheme for CFL equal or greater than the upper CFL limiter. Between those values a blending of both schemes is used. This correction is applied to improve robustness and stability when large time variation of the free surface shape is preset and the time step is too big to resolve it. After this correction $\tilde{\phi}_f^*$ experiences a final modification based on the interface angle, which is the angle θ between between the normal of the free surface interface $\mathbf{n}$ and the cell surface vector $\mathbf{S}_f$. This final modification reads:

$$\tilde{\phi}_f^{**} = \tilde{\phi}_f^* \left(\cos\theta\right)^{C_\theta} + \tilde{\phi}_C \left(1 - \cos\theta\right)^{C_\theta} \tag{5}$$

Here C_θ= represents an angle exponent. Its default value according to [9] is 0.05. The final cell face value is calculated as:

$$\phi_f^{HRIC} = \tilde{\phi}_f^{**} \left(\phi_D - \phi_U\right) + \phi_U \tag{6}$$

As a consequence of the modifications due to interface angle and local Courant number, the NVD can take different forms. For the three different blending states depending on local CFL, Figure 2 illustrates the possible forms of the HRIC scheme with respect to the interface angle θ. The areas shaded in red represent the possible forms the scheme can take depending on the angle factor for the respective local Courant number. This kind of blending strategy is more or less the same for all interface capturing schemes, so care has to be taken when modeling free surface flows to avoid unwanted switching to a lower resolution which is often accompanied with interface smearing.

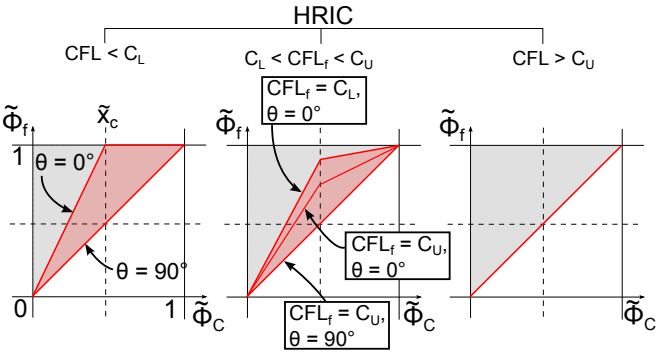

Figure 2: NVD of High Resolution Capturing Scheme (HRIC)

4 Theoretical Test Case

The theoretical review of the HRIC revealed that the encountered interface smearing is most probably related to the use of high Courant numbers. A modifier was found which implies that the HRIC scheme is used for a CFL smaller than the lower CFL limiter and UD scheme for CFL equal or greater than the upper CFL limiter. Between those values a blending of both schemes is used. From a theoretical point of view, the sole purpose of the correction of the HRIC scheme for local CFL is to improve robustness. If unsteady phenomena like slamming and or seakeeping are of interest, local Courant

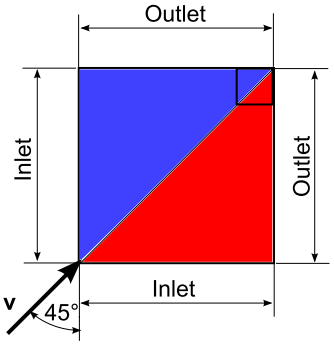

Figure 3: Sketch of test case setup

Number should be inherently lower than 0.5 anyway. If robustness is not problematic then this switch should be of no interest for calculation which seek a steady state solution. Since simulations mimicking towing tank procedures seek such a steady state solution, the HRIC scheme is modified such that the switch is effectively removed. If this assumption is true, this would remove the necessity to keep Courant number below 0.5 for even the smallest cell. The impact of this on practical applications is vast because it has the potential to significantly reduce computational effort by allowing larger time step sizes. To control the validity of this assumption a test case has been constructed. Aim of the test case is to produce a worst case scenario which makes it possible to judge if the modified differencing scheme can cope with the situation. From a theoretical point of view, the case which would produce the highest amount of numerical diffusion and thus the highest amount of interface smearing is a flow through a quadratic grid cell at an angle of $45°$. Therefore a 2D Cartesian grid has been build which consists of 128 x 128 grid cells with edge length of 0.5m. Total edge length of the domain is 64m. Initial volume fraction distribution is such that the lighter fluid (air) occupies the upper left triangle of the domain (blue) whilst the heavier fluid (water) is found in the lower right side (red). Inflow conditions for volume fraction have been set such that this state should remain within the simulation. Outlet has been set to Neumann conditions. A sketch of the setup is depicted in Figure 3. Depending on the local Courant number, the HRIC scheme switches between:

1. A pure HRIC scheme if CFL < 0.5
2. A linear between HRIC and UD scheme if $0.5 \leq$ CFL ≤ 1.0
3. A pure UD scheme if CFL > 1.0

The influence of these different states on the sharpness of the interface is tested by varying flow speed and time step size such that the relevant criteria is fulfilled. First, CFL is set to 0.3 resulting in a pure HRIC scheme (Figure 4a). Even though the flow direction with respect to cell faces is unfavorable, the HRIC scheme is able to resolve the sharpest interface possible within the VOF method (1 cell). Next the CFL is increased to 0.75, resulting in 50% blend between HRIC and UD (Figure 4b). This blend is also still sufficient to retain the sharp interface and therefore gives a valid solution. An explanation for this behavior can be found in the blending strategy depending on interface angle. As depicted in Figure 2, the difference between the pure HRIC and the blended HRIC is reasonably small for a cell flow angle of $45°$ which explains the similar results. Finally, flow speed and time step size of the unsteady simulation are set to values such that the Courant Number in the entire domain is 3.0. This leads to switching to a pure Upwind Differencing Scheme within the HRIC scheme. As a result the interface between air and water becomes severely smeared and is forming a cone-like shape starting from inlet towards outlet (Figure 4c). Now the HRIC scheme is modified by removing the CFL dependency. The Courant number is kept at 3.0 and the simulation repeated. Figure 4d illustrates the result which clearly shows that this modification allows using higher CFL numbers whilst a sharp interface is retained. This allows the conclusion that the modification of the HRIC scheme is well suited to simulate free surface flows at higher Courant numbers, allowing to converge faster towards a steady state solution.

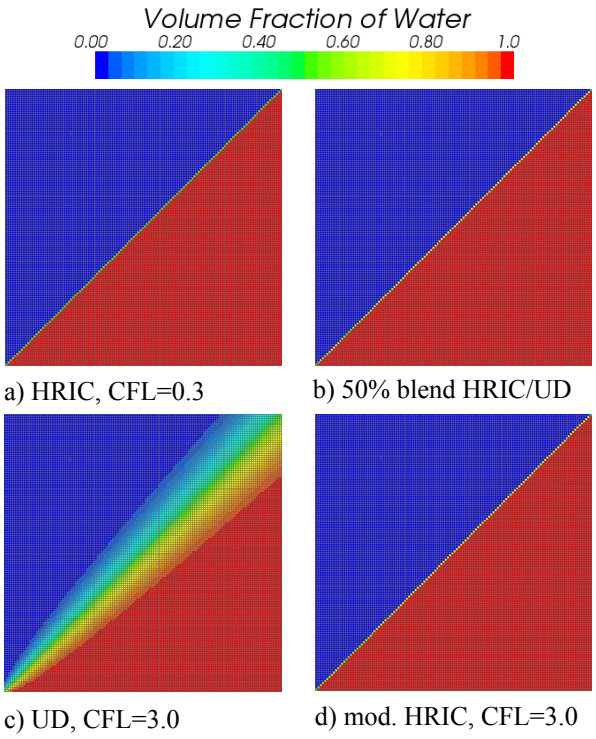

Figure 4: Impact of HRIC modes on free surface resolution

5 Validation & Verification against Towing Tank data

In most cases validations are conducted by comparing simulation results with trusted towing tank data. Deviations from experimental data are corrected by grid refinements until a acceptable agreement between EFD and CFD is found. However, this approach can lead to false confidence in the results if modeling or grid errors are present. Therefore, validation & verification are conducted here with a formal approach which allows to draw additional conclusions with respect to error types and error sources. First at all a short definition of the terms verification and validation is necessary:

- **Verification** includes the assessment of numerical uncertainty, magnitude and sign of numerical error (if possible) and uncertainty in error estimation.
- **Validation** is the assessment of uncertainty of the simulation model by means of experimental data plus the assessment of the modeling error itself.

The verification & validation procedure will be carried out in accordance with recommendations of the ITTC regarding *Uncertainty Analysis in CFD* [4]. For a detailed description see also Stern et al. [11, 12]. The simulation error δ_S is defined as the difference between simulation result S and reality

or truth T. It consists of the modeling error δ_{SM} and the numerical error δ_{SN}. Unfortunately δS can never be determined exactly since instead of T only experimental results are available which also contain a certain level of uncertainty.

$$\delta_S = S - T = \delta_{SM} + \delta_{SN} \tag{7}$$

For some cases magnitude and sign of the numerical error can be estimated, leading to corrected numerical uncertainty $U_{S_C N}$. For the uncorrected case only the numerical uncertainty U_{SN} is assessed. Therefore the numerical error δ_{SN} is decomposed into contributions from iteration number δ_I, grid size δ_G, time step δ_T and other parameters δ_P. With uncertainty U as described above this gives the following expression:

$$U_{SN}^2 = U_I^2 + U_G^2 + U_T^2 + U_P^2 \tag{8}$$

For validation purpose the comparison error E between the benchmark experimental data D and the simulation result S is determined in order to asses modeling uncertainty U_{SM}.

$$E = D - S = \delta_D - (\delta_{SM} + \delta_{SN}) \tag{9}$$

To determine if validation of a value has been achieved, comparison error E is compared with the validation uncertainty U_V.

$$U_V^2 = U_D^2 + U_{SN}^2 \tag{10}$$

If $|E| < U_V$, than the combination of all errors in both simulation and experimental data is smaller than the validation uncertainty. Then validation has been achieved for this validation uncertainty level. In the case that $U_V << |E|$, the modeling error δ_{SM} can be used to achieve modeling improvements.

5.1 Verification Procedure

In the course of the verification process a grid convergence study has to be conducted. In order to do this it is necessary to use a minimum of three grids which have been uniformly refined with an increment Δx_k such that constant refinement ratio r_k exits.

$$r_k = \frac{\Delta x_{k_2}}{\Delta x_{k_1}} = \frac{\Delta x_{k_2}}{\Delta x_{k_2}} = \frac{\Delta x_{k_m}}{\Delta x_{k_{m-1}}} \tag{11}$$

ITTC Guidelines recommend refinement ratio r_k between $\sqrt{2}$ and 2. Throughout this work ratios of 1.5 and 2 have been used. Next a convergence ratio R_k is defined to give information about convergence respective divergence of a solution. It is defined as follows:

$$\begin{aligned} \epsilon_{21_k} &= S_{k_2} - S_{k_1} \\ \epsilon_{32_k} &= S_{k_3} - S_{k_2} \\ R_k &= \epsilon_{21_k} / \epsilon_{32_k} \end{aligned} \tag{12}$$

with ϵ_{ijk} as the solution changes for the input parameter k between three solutions ranging from fine S_{k_1} to coarse S_{k_3}. According to the ITTC guidelines [4], three different cases are distinguished:

$$\begin{aligned} &(i) \text{ Monotonic convergence: } 0 < R_k < 1 \\ &(ii) \text{ Oscillatory convergence: } R_k < 0^i \\ &(iii) \text{ Divergence: } R_k > 1 \end{aligned} \tag{13}$$

In the case of (i) the Generalized Richardson Extrapolation is used to assess the uncertainty U_k or the error estimate $\delta_k^\star$ and the corrected uncertainty U_{k_C}. For oscillatory convergence (case (ii)) the uncertainty U_k is estimated by determining the error between minimum and maximum of the oscillation. In the case of divergence (iii) it is not possible to estimate errors or uncertainties.

5.1.1 Generalized Richardson Extrapolation

As stated above, in case of monotonic convergence generalized RE is used to determine the error $\delta_k^\star$ with respect to refinement ratio r_k and order-of-accuracy P_k. Usually $\delta_k^\star$ is estimated for the finest solution of the input parameter $m = 1$ only. With number of available solutions $m = 3$ only the leading-order term of the error may be evaluated. This gives the following equations for $\delta_k^\star$ andP_k.

$$\delta_{k_1}^\star = \delta_{RE_{k_1}}^\star = \frac{\epsilon_{21_k}}{r_k^{p_k} - 1} \tag{14}$$

$$p_k = \frac{ln\left(\epsilon_{32_k}/\epsilon_{21_k}\right)}{ln\left(r_k\right)} \tag{15}$$

Unless the solution is in the asymptotic range, equation (15) only gives a poor estimation of the order-of-accuracy. Therefore a correction factor C_k is used to include the effect of higher-order terms priory neglected. C_k is defined as follows:

$$C_k = \frac{r^{P_k} - 1}{r^{P_{kest}} - 1} \tag{16}$$

The corrected error $\delta_{k_1}^\star$ is defined by combining equations (14) and (16)

$$\delta_{k_1}^\star = C_k \delta_{RE_{k_1}}^\star = C_k \left(\frac{\epsilon_{21_k}}{r_k^{p_k} - 1} \right) \tag{17}$$

Depending how close the corrected error $\delta_{k_1}^\star$ is to the asymptotic range (how close C_k is to 1) the expression to assess the uncertainties take different forms. If C_k is sufficiently greater than one and lacking confidence only U_k is estimated by the following formula:

$$U_k = \left| C_k \delta_{RE_{k_1}}^\star \right| + \left| (1 - C_k)\, \delta_{RE_{k_1}}^\star \right| \tag{18}$$

For C_k being sufficiently smaller than one the ITTC recommends to use expression (19) to assess U_k.

$$U_k = \left| \delta_{RE_{k_1}}^\star \right| + 2 \left| (1 - C_k)\, \delta_{RE_{k_1}}^\star \right| \tag{19}$$

If C_k is sufficiently close to 1, the error $\delta_k^\star$ can be estimated. This allows to determine a corrected solution S_C and a thus a corrected uncertainty U_{k_C}.

$$U_{k_C} = \left| (1 - C_k)\, \delta_{RE_{k_1}}^\star \right| \tag{20}$$

5.2 Validation Procedure

As stated in section 5, validation is defined as a process to the model uncertainty U_{SM} and, if possible, sign and magnitude of the modeling error δ_{SM} itself. This is done by using experimental data to compare the simulation results with. Thus the error in the experimental data has to be considered, making it easier to validate simulations if the experimental error is large. It must thus be noted that the level of validation is strongly depended on the quality of the comparison data. The validation procedure is based on the relation between validation uncertainty U_V, predefined programmatic validation requirement U_{reqd} and comparison error $|E|$. These three variables may form the following six combinations:

$$\begin{aligned} |E| < U_V < U_{reqd} \\ |E| < U_{reqd} < U_V \\ U_{reqd} < |E| < U_V \\ U_V < |E| < U_{reqd} \\ U_V < U_{reqd} < |E| \\ U_{reqd} < U_V < |E| \end{aligned} \tag{21}$$

In cases 1 - 3 of (21) the results are validated. Validation is achieved at the level of validation uncertainty U_V. This means that the comparison error is below the noise level resulting in an impossibility to estimate error due to modeling assumption δ_{SMA}. In the case of 1, the validation level is also below U_{reqd} which makes the validation successful from a programmatic point of view. For case 4- 6 the comparison error is above the noise level. Sign and magnitude of E can be used to estimate δ_{SMA}. In the fourth case the validation is achieved at $|E|$ level with respect to the used software.

5.3 Grid Convergence Studies on ACCV5 boat for non-lifting cases

Verification and validation is performed on the geometry of Americas Cup Class Version 5 boat (ACCV5) for which experimental towing tank data is available. These boats have a rather complex geometry which besides hull, keel fin and rudder also includes a trim tab for the keel and a ballast bulb with wings. Since model scale λ=3, which is rather close to full scale compared with tank models for conventional vessels, it was decided that it is possible to do the validation in full scale. Therefore experimental data have been transformed to full scale by employing a modified version of the ITTC procedures. The modifications applied mainly consist of own friction coefficients and form factor (1+k) values for yacht appendages. The conditions of the calculations are a Froude number Fn of 0.403 and normalized Reynolds number Rn of 4.75×10^6. The boat is allowed to sink dynamically, but not to pitch. The pitch angle is prescribed at $\psi = 0.46$ bow down trim. *STAR-CCM+7.02.008* is used as flow code to solve the Reynolds-Average-Navier-Stokes equations for the flow field around the yacht. The simulation is conducted at fully turbulent conditions and the $k - \omega$ based *Shear Stress Transport (SST)* model has been used to model turbulence.

5.3.1 Computational Grids

Grid Convergence studies have been conducted using 3 different combinations of refinement parameters to study their impact on grid densities and computational results. The computational grid has been modeled such that it depends on one *base number*. This way it can be ensured that a constant grid refinement ratio r_k is used. Two exceptions from this modeling paradigm exist. First the prism layer used to resolve the boundary layer around hull and appendages is excluded from refinement because this would lead to large changes in dimensionless wall-scale Y^+. Most likely this would lead to changes in near-wall treatment like using a low-Reynolds approach for one simulations and wall functions for the other. This would render the simulations incomparable. Therefore the total thickness of the prism layer, the thickness of the wall nearest node and the number of prism layers are kept constant throughout this verification & validation. The second exception concerns the resolution of the free surface. Since free surface resolution is very important for correct resolution of ship drag, it has been given its own base number. This way it is possible to evaluate the influence of different refinement ways on both computational grid and solution. The refinement ways investigated within this work are:

1. *Global refinement*; were only the global grid base number is refined.
2. *Free Surface refinement*; were only free surface parameters are refined by their base number. Free surface refinements consists of a vertical refinement in the whole domain at the expected level of the wave pattern and a second refinement in both longitudinal and traversal direction in the vicinity of the Kelvin pattern.
3. *Overall refinement*; were both global and free surface base number are modified as a function of the refinement ratio r_k.

For all three cases four grids with constant refinement ratio $r_k = 2$ have been constructed. Resulting grid sizes varied from 8.1×10^5 cells for the coarsest grid to 1.2×10^7 for the finest.

5.3.2 Verification and Validation of Resistance

The verification of resistance has been performed with respect to grid convergence. Iterative convergence has been taken into account, but since it was in the order of 0.05% C_T it was considered neglectable. The results of the studies have been summarized in table 1 and 2. Table 1 illustrates the C_T values for the different grids as well as the solution change ϵ from a coarser to a finer solution between adjacent grids. Here ϵ is defined as:

$$\epsilon = \frac{(S_i - S_{i+1})}{S_{i+1}} \tag{22}$$

The results show that the changes of C_T between the different solutions are largest in the case were free surface parameters variations are involved (Case 2-3). Verification results are illustrated in table 2. Here convergence ratio R_G indicates

Table 1: Grid convergence study for total resistance $C_T\ (\times 10^{-3})$ for ACCV5

		Grid Number				
Nr.	Var	4	3	2	1	EFD
1)	C_T	6.46	6.33	6.29	6.28	6.32
	ϵ		-2.0%	-0.6%	-0.2%	
2)	C_T	5.87	6.02	6.19	6.28	6.32
	ϵ		2.6%	2.7%	1.5%	
3)	C_T	6.06	6.05	6.24	6.28	6.32
	ϵ		-0.1%	3.1%	0.6%	

$\%S_G$

Table 2: Verification of total resistance $C_T\ (\times 10^{-3})$ for ACCV5

Nr.	Grid	R_G	U_G	$\delta_G^\star$	S_C
1)	1-3	0.34	0.11%	0.07%	-0.07%
	2-4	0.30	0.26%	0.20%	0.01%
2)	1-3	0.58	2.06%	-0.50%	0.5%
	2-4	1.08	-	-	-
3)	1-3	0.20	0.25%	-0.20%	0.2%
	2-4	-40.39	-	-	-

$\%S_G$

monotonic grid convergence of solutions for grids 1-3 for all three case ($R_G < 1$). For the coarser grid sequence (grids 2-4) only case 1 (Global refinement) shows monotonic convergence. For the coarser grid sequence of the free surface refinement study (case 2) R_G indicates divergence whilst for the same grid sequence of the global refinement study (case 3) the solution appears to be of oscillatory nature. However, the later indicator seems to be misleading, so results for case 3.b are also treated as divergent. It is therefore not possibly to estimate error or uncertainty for case 2.b and 3.b. Where appropriate Generalized Richardson Extrapolation is used to estimate sign and magnitude of the grid error $\delta_G^\star$ and a corrected uncertainty U_{G_C} as well as a corrected solution S_C (equations (14) - (20)). The thus gained corrected solution can be compared to the solution S_G. This gives an estimation of the level of verification of the simulation. In all cases were an estimation of the numerical uncertainties was possible, the corrected solution does not differ much from the originally calculated with differences in the range of -0.07 to 0.5%S_G. It can thus be concluded that in all those cases the level of verification is rather good and the results can be considered verified. Validation of the simulation results is performed with respect to the results of the towing tank tests. Therefore the comparison error is calculated according to equation (9) taking into account the simulation result S and the experimental data D. In order to conduct the validation as defined in (21), the validation uncertainty U_V has to be calculated (10). The corrected comparison error E_C is defined as in (9) but using S_C instead of S. Table 3 summarizes comparison error E,

Table 3: Validation of total resistance $C_T\ (\times 10^{-3})$ for ACCV5

Nr	Grid		$E\%$	$U_V\%$	$U_D\%$	$U_{SN}\%$
1)	1-3	E	0.6	2.0	2.0	0.11
		E_C	0.7	3.2	2.0	0.04
	2-4	E	0.4	2.0	2.0	0.26
		E_C	0.6	3.2	2.0	0.05
2)	1-3	E	0.6	2.9	2.0	2.04
		E_C	0.1	4.1	2.0	1.55
	2-4	E	2.1	-	2.0	-
		E_C	-	-	2.0	-
3)	1-3	E	0.6	2.0	2.0	0.25
		E_C	0.4	3.2	2.0	0.05
	2-4	E	1.2	-	2.0	-
		E_C	-	-	2.0	-

$\%D$

validation uncertainty U_V, experimental uncertainty U_D and simulation uncertainty U_{SN} as percentage of D for both corrected and uncorrected approaches. It has to be noted that data uncertainty U_D has not been specified in the experimental towing tank data. Details regarding experimental uncertainties of large towing tank facilities are rarly found in literature. Longo and March [7] give values between 0.6% - 1.5% for a systematic investigation of the surface combatant DTMB 5415 model with respect to experimental errors whilst Yan et al. [13] give values of 2.8% for the same ship. Similar data for yacht investigation have not been available. The only source found for uncertainties of yacht investigation has been a presentation given by Frank DeBord at Stevens Institute [2]. The data given in this presentation show the long term repeatability of towing tank tests to be approximately 3%. Also this overview of towing tank uncertainties is by no means complete, it can be concluded that the data uncertainty normally should not exceed 3%. It was therefore decided that it is feasible to take into account a experimental uncertainty U_D of 2% for validation purpose. By comparing E and U_V of table 3 one can easily see that for all cases in which the comparison error could be calculated, $E < U_V$ is true. Therefore results have been validated for all cases except case b (grids 2- 4) of both free surface and overall refinement studies. This coincides with the findings of the verification study and allows the conclusion that both verification & validation has been achieved for all refinement studies except the two cases stated above. The formal validation and verification procedure as conducted above only allows to draw conclusion regarding the finest grid in the study, in this case grid 1 respective grid 2. Whilst not giving the same level of certainty a plot of results deltas over grid cells is a feasible approach to judge the sensitivity of the solution to grid changes. Figure 5 illustrates resistance coefficient ΔC_T over grid points. It is interesting to note that with ongoing refinement cases including free surface grid parameters show an increasing drag whilst for the general refinement case the opposite holds true. The later one coincides with the

widely held doctrine that with ongoing refinement a RANSE solution gives smaller forces until grid invariance of results is reached. This investigations suggest that while this certainly holds true for single phase investigation of deeply submerged bodies, it is not applicable to free surface flows around floating bodies. The rationale behind this behavior probably is that a too coarse resolution of free surface leads to increased wave damping thus altering the pressure fluctuations on the hull such that a lower wave resistance is predicted. However, to be sure this theorem would have to be proofed. The distribution of results also illustrates the high impact of free surface refinement parameters on overall grid density and result accuracy. It can be concluded that special attention has to be devoted to these parameters in order to achieve reliable results.

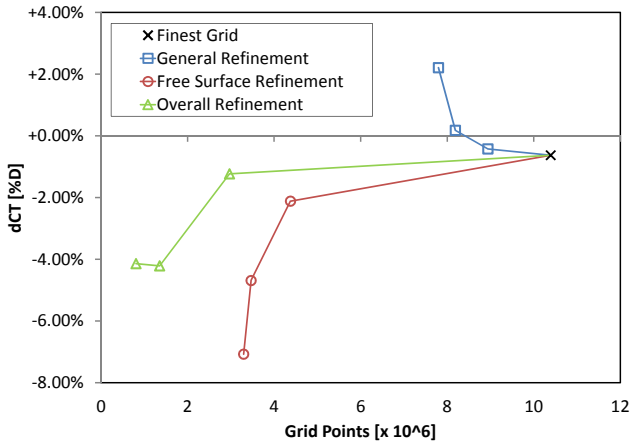

Figure 5: ΔC_T over Grip Points w.r.t to Experimental Data

Since the correct determination of wave resistance is crucial for reliable results on total resistance of ships, a refinement study for free surface flows also has to take into account its influence on generated wave patterns. Figure 6 compares wave resolution from initial studies (top) with results gained with the modified HRIC scheme.The top picture shows that the computational domain is too short and the wave patterns is diffuse and damped. Especially the later suggests an insufficient resolution of the free surface. The bottom of figure 6 shows the finest grid of the investigation. Obviously there are large differences between the two simulations, the later one showing a sharp resolution of primary and secondary wave trains. Here wave damping seems to be largely reduced.

One of the goal of this investigation was to reduce numerical ventilation caused by the smearing of the free surface interface. Figure 7 shows the volume fractions of water at the yacht surface for the old approach with Courant number dependency whilst figure 8 illustrates the same for the new approach without. Comparing the two cases one can clearly see from the profile view that the new approach gives a much sharper interface between air (blue) and water (red). The differences are most distinctive at the bow wave which takes an entirely different shape. The bow wave of the old approach (figure 7) has a large region over which the interface is smeared and this smearing is transported significantly down-

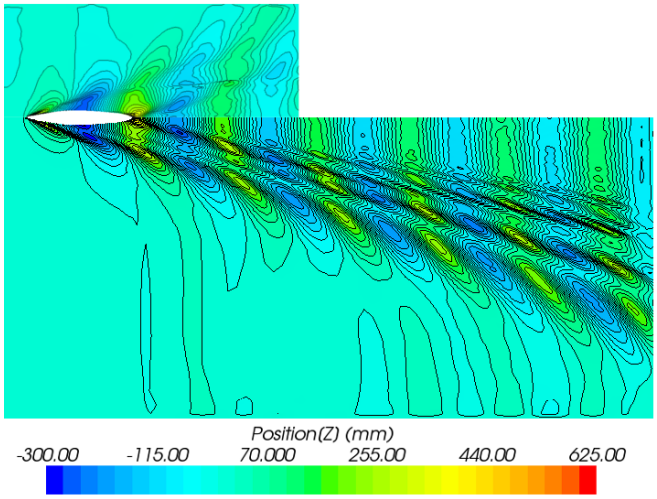

Figure 6: wave contours from *initial studies* (top) and from *Grid Convergence* studies (bottom, grid 1 - finest grid)

stream. For the new approach (figure8) the bow wave is much more distinctive and the free surface interface is usually captured over 3-4 cells. This clearly shows an advantage of modified approach over the old. However, plan view reveals that the volume fraction achieved with the new approach still is not perfect. Whilst the improvements between old approach and new approach are obvious and pleasant, plan view still reveals some remaining interface smearing. Still the improvement is large since the volume fraction for the old approach ranges between 0.4 and 1.0, whilst for the new approach the range is between 0.85 and 1.0. It seems that within the VOF method achieving perfect results without smeared interfaces for this rather blunt bows is still very hard if not impossible. Nonetheless from an engineering point of view the simulation is absolutely applicable since with respect to the verification & validation results the error in total resistance is small.

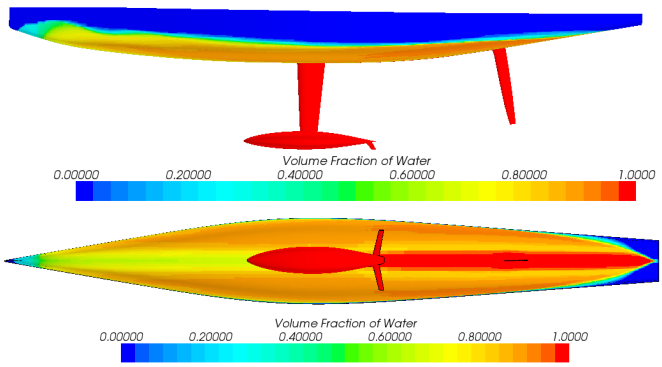

Figure 7: Numerical Ventilation with Courant Number dependency

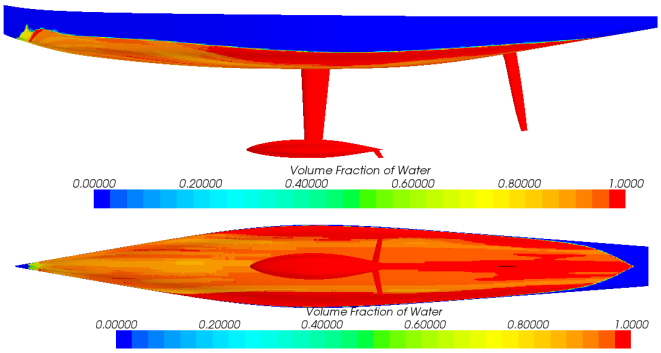

Figure 8: Numerical Ventilation *without* Courant Number dependency

5.4 Grid Convergence Studies including Lift

After the successful verification & validation of the point variable C_T for the sailing yacht in upright conditions reported in section 5.3, a further study has been conducted in order to proof the feasibility of the approach for heeled conditions of the yacht. Heeled conditions include the generation of hydrodynamic lift by the yacht and its appendages. Therefore a validation & verification for these conditions cannot be restricted to the evaluation of total resistance C_T. Instead it has to include the lifting component to consider the complete state of the yacht. Therefore the two point values total drag coefficient C_D and total lift coefficient C_L are evaluated together. The correct evaluation of this forces within towing tank experiments or CFD simulations requires the modeling of aerodynamic forces which a sailing yacht encounters. In order to correctly simulate the influence of the aerodynamic force generated by the sails, one has to introduce an additional dynamic sail trimming moment around the y-axis of the yacht which is equal to hydrodynamic drag D times the vertical center of efforts of the sails VCE_{aero}.

$$M_{Y_{dyn}} = D \cdot VCE_{aero} \tag{23}$$

Additionally, the generation of lift by the yacht hull and appendages introduces a vertical force pointing up. Similar to the trimming moment explicated above, this force has to be countered by a collinear aerodynamic vector of equal length and different sign. This sail force has to be modeled during testing as a additional dynamic sink force $F_{Z_{dyn}}$. It is modeled as heeling force F_H times the sine of the heeling angle ϕ.

$$F_{Z_{dyn}} = F_H sin\phi \tag{24}$$

Contrary to the upright resistance grid convergence study, this study has been conducted in model scale. This approach not only allows easier comparison between results but also makes the appliance of the various additional input parameters easier. Whilst for the non-lifting test cases validated in section 5.3 trim was kept fixed and only sinkage was dynamically calculated, the present case sets both state variables free. This is a major change since it makes it necessary to account for similar trim and sinkage forces in order to compare simulation and experiment. For the towing tank experiment prescribed trim moments and vertical forces exist as input values. These values have been used as input data for the CFD simulation instead of dynamic calculation of these values, which would also have been possible.

5.4.1 Computational Grids

The grid convergence study has also been conducted according to ITTC standards as explicated in section 5.3. The principal design of the grids is identical to the one used in section 5.3. It includes refinement of the free surface in vertical direction and additionally in horizontal dimensions in the vicinity of the kelvin angle around the boat. The results of the non-lifting verification & validation study clearly showed that the major factor towards a grid independent solution is the refinement of the free surface. Figure 5 illustrates that surface grid refinement is already sufficient. Therefore only free surface refinement has been varied for the present grid convergence study. Grid parameters have been systematically varied according to table 4. In contrast to the grid convergence study for the non-lifting case in section 5.3 the constant grid refinement factor has been decreased from 2 to 1.5. This has been done to get a more uniform refinement in terms cell sizes which enhances the comparability of the results. The

Table 4: Grid Parameter for Grid Invariance Study

Ref. Factor (-)	Interface Spacing dz (mm)	dx & dy (m)	Grid Size (-)
1.0	10.0	0.0625	1.25×10^7
1.5	15.0	0.0938	7.07×10^6
3.0	22.5	0.1406	3.57×10^6

differences of lift and drag coefficient to the experimental data derived from the grid convergence study is shown in figure 9. The figure illustrates that the drag coefficient C_D is always underestimated, whilst for the lift coefficient C_L the contrary holds true. However, differences to EFD are rather low for both coefficients and in the same order of magnitude. Generally both coefficients converge quite satisfactorily, giving the first indication of a high quality solution. Table 5 gives the numerical values of the convergence of drag, lift and lift/drag-ratio. The solution change from a coarser to a finer solution ϵ, as defined in (22), decreases continuously. The results of the verification procedure (table 6) show that the convergence ratio $R_G < 1$ is true for all cases, allowing the conclusion that the decrease is monotonic for all values. The biggest uncertainty of the computational grid U_G is 0.52% for the lift-to-drag ratio C_L/C_D which is already very low. Since the convergence is monotonic, it is possible to use *Generalized Richardson Extrapolation* in order to apply a correction for numerical error. In particular, it is possible to calculate a correct grid uncertainty U_{G_C} and a corrected solution S_C. With a maximum derivation of 0.14%, these corrected values are even closer to the experimental values. It can be generally said that from a numerical point of view the results of the grid convergence study show a docile behavior and steadily

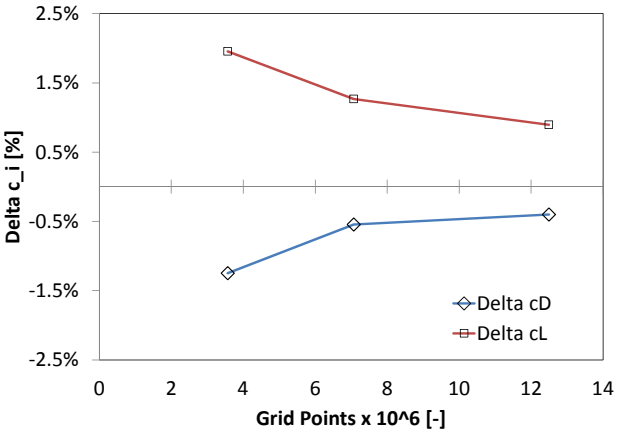

Figure 9: ΔC_i over Grid Points

Table 5: Grid Convergence of drag and lift for ACCV5

	Grid 3	Grid 2	Grid 1	EF Data
C_D	8.94	9.00	9.01	9.05
ϵ	-	0.7%	0.1%	
C_L	1.89	1.88	1.87	1.86
ϵ	-	-0.7%	-0.4%	
C_L/C_D	2.12	2.09	2.08	2.05
ϵ	-	-1.4%	-0.5%	

$\%S_G$

converge towards the experimental values with increasing refinement. This allows the conclusion that the simulation is verified. Table 7 gives an overview of the values necessary for

Table 6: Verification of drag and lift for ACCV5

Variable	R_G	U_G	$\delta^\star_G$	U_{G_C}
C_D	0.21	0.19%	-0.12%	0.08%
C_L	0.54	0.44%	0.30%	0.14%
C_L/C_D	0.37	0.52%	0.41%	0.11%

$\%S_G$

the validation procedure. Data uncertainty U_D and numerical simulation uncertainty U_{SN} are combined to the validation uncertainty U_V. $U_V$is then compared to the comparison error E_C which is defined as data D minus simulation result S as per equation 9. The table list all values both for the uncorrected solution and the solution corrected by means of Generalized Richardson Extrapolation. Per definition, a simulation is validated if the comparison error is less or equal the validation uncertainty. This clearly the case for all six comparison cases. The simulation can therefore be considered validated at validation uncertainty level.

It can be summarized that verification & validation for lifting conditions was highly successful. Achieved results are not

Table 7: Validation of drag and lift for ACCV5

Variable		$E\%$	$U_V\%$	$U_D\%$	$U_{SN}\%$
C_D	E	0.4%	2.0%	2.0%	0.19%
	E_C	0.3%	2.0%	2.0%	0.08%
C_L	E	-0.9%	2.0%	2.0%	0.44%
	E_C	-0.6%	2.0%	2.0%	0.15%
C_L/C_D	E	-1.3%	2.1%	2.0%	0.53%
	E_C	-0.9%	2.0%	2.0%	0.11%

$\%D$

only considerably below validation uncertainty level but also very close to experimental data. Although this formally does not decrease the uncertainty of the results, it still increase the confidence in the applied methods. It also shows again that the assumptions regarding free surface interface smearing made in the previous sections are correct.

6 Summary

The motivation for this investigation has been a failed first attempt to correctly determine total resistance of free surface flow around an ACCV5 hull. A review of the first simulations led to the assumption that the problem could be traced back to the occurrence of extensive interface smearing at the yacht hull. This led to a thorough review of the theory behind the interface capturing model in section 3. This review showed that the problems encountered most likely were situated in the use of Courant numbers exceeding 0.5, thus causing the switch to a 1st order upwind differencing scheme. Since reducing the overall time step size such that it would allow the maximum Courant number to be lower than 0.5 would lead to undesirable long simulation times an alternative approach was sought to allow the use of higher order schemes like e.g. the HRIC scheme within acceptable time step size. It was concluded that it might be possible to modify the VOF model such that it does not switch to upwind differencing even if the local Courant number would be larger than 0.5. This approach seems feasible as long as only a steady state solution is sought-after. Section 4 shows a numerical test case which allows the conclusion that this approach is feasible. Therefore, the modified scheme was applied to the simulation of the total resistance of the ACCV5 yacht. Verification and Validation according to the ITTC guidelines was then conducted against experimental data for lifting and non-lifting test cases. Extensive grid studies have been carried out, thus also allowing to judge the sensitivity of the results to the change of various grid parameters. The results showed a much sharper capturing of the free surface interface with the new approach. It was also shown that the initial differences in overall resistance were mainly caused by the poor free surface resolution caused by the interface smearing. This interface smearing caused a numerical damping of the waves resulting in a wave resistance which was too small. The grid convergence studies clearly showed that the free surface simulations for yachts are more sensible to free surface resolution and thus to wave resistance

than they are to yacht surface resolution (friction and pressure forces). Overall it can be concluded that the use of the higher order scheme which was made possible by the modification of the existing implementation led to large improvements and a successful verification & validation. It has to be stressed that the new approach with the modified scheme is only valid if one is interested in a steady solution. It was also shown that the simulation still suffers from a small amount of interface smearing, however the overall effect on the results may be considered as small. Generally, the error in verification & validation was satisfying small.

REFERENCES

[1] C. Böhm and K. Graf. Validation of ranse simulations of a fully appended accv5 design using towing tank data. In *International Conference on Innovation in High Performance Sailing Yachts*, Lorient, France, April 2008.

[2] Frank DeBord. Hydrodynamic performance prediction for grand prix sailing yachts. Presentation at Stevens Institute.

[3] C Hirt and B Nichols. Volume of fluid (vof) method for the dynamics of free boundaries1. *Journal of Computational Physics*, 39(1):201–225, 1981.

[4] ITTC. *ITTC Recommended Procedures and Guidelines; Uncertainty Analysis in CFD; Verification and Validation*. International Towing Tank Conference, 2008.

[5] Lars Larsson, Frederick Stern, and Michel Visonneau. *Gothenburg 2010, A Workshop on Numerical Ship Hydrodynamics*. Chalmers University of Technology, 2010.

[6] B. P. Leonard. Simple high-accuracy resolution program for convective modelling of discontinuities. *International Journal for Numerical Methods in Fluids*, 8(10):1291–1318, 1988.

[7] Joe Longo and Fred Stern. Uncertainty assessment for towing tank tests with example for surface combatant dtmb model 5415. *Journal of Ship Research*, 49, No.1:55–68, March 2005.

[8] S. Muzaferija and M. Peric. Computation of free-surface flows using the finite-volume-method and moving grids. *Numerical Heat Transfer, Part B: Fundamentals*, 32(4):369–384, 1997.

[9] S. Muzaferija and M. Peric. *Computation of free surface flows using interface-Tracking and interface-capturing methods*, chapter 2, pages 59–100. Computational mechanics publications. WIT Press, Southampton,, nonlinear water wave interaction edition, 1999.

[10] S. Muzaferija, M. Peric, P. Sames, and T. Schellin. A two-fluid navier-stokes solver to simulate water entry. In *Twenty-Second Symposium on Naval Hydrodynamics*, Washington D.C:, 1999.

[11] Fred Stern, Robert Wilson, and Jun Shao. Quantitative v&v of cfd simulations and certification of cfd codes. *International Journal for Numerical Methods in Fluids*, 50(11):1335–1355, 2006.

[12] Fred Stern, Robert V. Wilson, Hugh W. Coleman, and Eric G. Paterson. Comprehensive approach to verification and validation of cfd simulations—part 1: Methodology and procedures. *Journal of Fluids Engineering*, 123(4):793–802, 2001.

[13] Kai Yan, Feng Zhao, Cheng sheng Wu, and Lei Yang. Numerical and experimental uncertainty analysis for the prediction of resistance and wave profile of a surface ship model. In *8th International Conference on Hydrodynamics*, 2008.

7 AUTHORS BIOGRAPHY

Christoph Böhm holds a diploma degree in naval architecture from the University of Applied Sciences Kiel. He is currently working as a flow scientist at the Yacht Research Unit Kiel. He is specialized on RANSE simulations of sailing yacht appendages and hulls as well as subsequent VPP integration. He is currently working towards his PhD thesis at TU Delft.

Kai Graf is professor for ship hydrodynamics at the University of Applied Sciences Kiel and senior scientist of the Yacht Research Unit Kiel. Kai is working on sailing yacht aero- and hydrodynamics since 1998, being specialized on numerical simulation methods.